Parallel Operation of Grid-forming Inverters with Synchronous Machines

**T. THILEKHA[1]*, S. FILIZADEH[1], U. ANNAKKAGE[1], D. MUTHUMUNI[2],
C. KARAWITA[3]**
University of Manitoba[1]
Manitoba Hydro International[2]
Transgrid Solutions[3]
Canada

SUMMARY

The virtual synchronous machine (VSM) concept is a common grid-forming inverter control method, which is used to control a converter by emulating different levels of the mechanical and electrical characteristics of a synchronous machine (SM). Virtual inertia to support inertial response, virtual active power-frequency (*P-f*) droop for primary frequency control, and virtual reactive power-voltage (*Q-v*) droop for primary voltage control are integrated into the VSM controller used in this work. These basic functionalities ensure proper operation during normal conditions. Under abnormal conditions, such as during a fault, low thermal limits of power electronic switches hinder the fault-ride-through capability of the converter. The inclusion of a current controller is a cost-effective solution and there exist several current limiting algorithms. Current controllers that maintain the voltage-source mode of operation during the fault preserve the converter's grid-forming capability. Therefore, this work uses a virtual impedance-based current controller that remains in the voltage source mode. The local measurement-based droop controller method does not demand a robust communication system and is, therefore, used in this study to enable the parallel operation of grid-forming inverters. The differences in bandwidths of *P-f* and *Q-v* control loops of VSM and SM determine their transient responses. This paper investigates the parallel operation of grid-forming inverters and conventional SMs using detailed switching models in the PSCAD/EMTDC simulator. The response to a balance three-phase fault at the point of interconnection (POI) is studied under different inverter penetration levels. The impact of inertia of the VSM and SM on fault-ride-through is also discussed. The adopted current-controller performance, particularly when riding through a fault with a SM is closely studied. This study shows the possible ways of improving the parallel operation of grid-forming inverters and conventional SMs under normal and faulted conditions.

KEYWORDS

Virtual synchronous machines (VSMs), synchronous machines (SMs), parallel operation, fault response, inertia, droop coefficient.

muthukut@myumanitoba.ca

1. INTRODUCTION

Presently integration of inverter-tied resources requires them to coexist with conventional synchronous machines (SM). The absence of inherent inertia, low current-carrying capability of the power electronic switches, harmonic injection, and intermittency of the primary energy source are the key challenges put forward by the inverter-tied resources compared to a SM. The virtual synchronous machine (VSM) controller is used to control the inverter as a grid-forming inverter to ensure gird-connected and islanded modes of operation. The virtual impedance-based current-limiting method, which preserves the voltage source characteristics even during the current limiting mode is used in this work. An ideal dc side is assumed for the inverter; therefore, this study does not investigate the impact from the dc side dynamics. The parallel operation of grid-forming inverters with SM is investigated while specifically focusing on their fault-ride through capability.

The next section discusses the test system and control scheme used in this study. Section III elaborates the impact of control and network parameters on the fault-ride through capability of a parallelly connected grid-forming inverter and a SM using PSCAD/EMTDC simulation results. The final section draws conclusions from the study.

2. TEST SYSTEM

To study the parallel operation of a grid-forming inverter and a synchronous machine, the test system given in Fig. 1 is developed in PSCAD/EMTDC. The test system consists of a three-phase, two-level
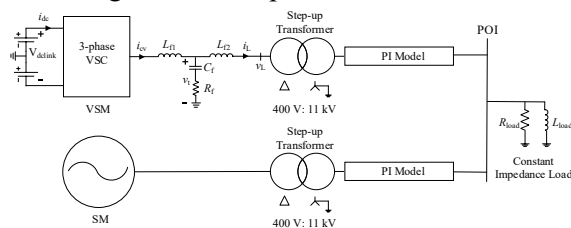

Figure 1 The single-line diagram of the test system

voltage source converter (VSC) connected to the POI via an LCL filter, a step-up transformer, and a 10 km long transmission. The VSC is controlled as a grid-forming inverter. The LCL filter is tuned to maintain the total harmonic distortion (THD) of the converter current below 5%. The model available in PSCAD/EMTDC is used to represent the conventional SM. The simplified governor model and non-reheat type turbine model available in [1] are used for the primary frequency control of the SM. The ACA4 exciter model is developed for the SM terminal voltage control. The governor, turbine, and the exciter models are appropriately initialized using the back-initialization approach. SM model parameters are mentioned under section *2.2* and the rest of the network parameters are given in Tables I and II.

Table I The Parameters of the Test System

Parameter	Value	Parameter	Value	Parameter	Value	Parameter	Value
S_{rated}	500 kVA	V_{dclink}	820 V	L_{f1}	150 μH	L_{f2}	30 μH
R_{load}	172.857 Ω	L_{load}	0.917 H	C_f	828.93 μF	R_f	0.09526 Ω
L_{tf}	0.1 pu	R_{tf}	0.01 pu				

Table II The Parameters of the Transmission Line Model

Positive-sequence parameters	Negative-sequence parameters
R=0.103 Ω/km, X_L=0.405 Ω/km, X_C=4.117 μs/km	R=0.279 Ω/km, X_L=1.802 Ω/km, X_C=2.414 μs/km

2.1 Grid-Forming Controller

The grid-forming controller topology is given in Fig. 2. The active power-frequency (*P-f*) controller, which consists of the *P-f* droop and the swing equation path generates a virtual rotor angle, θ [2]. The reactive power-voltage (*Q-v*) controller is based on the *Q-v* droop relationship and generates the reference q-axis converter terminal voltage (v_{tq}*) [3]. The virtual impedance (VI) based current controller provides current limiting via the current-dependent VI path and damping to any oscillations in the converter current following a disturbance, using the transient VI path [4].

The current-dependent VI path activates only if the converter current magnitude ($i_{\text{cv\_rms}}$) is higher than the set threshold current ($i_{\text{threshold}}$). In such instances this current difference is multiplied by proportional gains K_{pRVI} and K_{pLVI} to obtain the magnitudes of the current-dependent virtual resistance (R_{vi}) and virtual inductance (L_{vi}), respectively. These values are then multiplied by the corresponding dq components of the converter current (i_{cvdq}). The transient VI path does not contribute during steady operation. Following a disturbance, non-zero high-pass-filtered converter current components (i_{cvdqhp}) are present. These current components are multiplied by constant virtual resistance (R_{vi0}) and virtual inductance (L_{vi0}) values. Both these paths emulate a variable virtual impedance placed between the converter terminal and the filter inductance. The control parameters used in the study are tabulated in Table III.
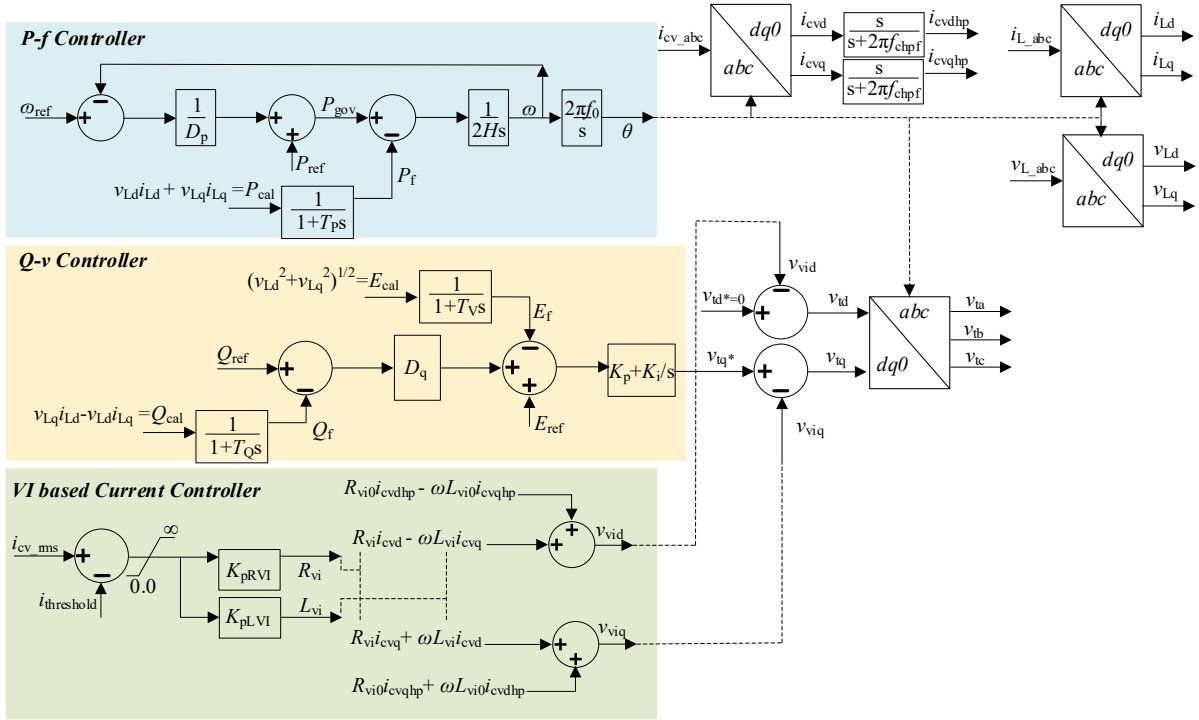

Figure 2 The grid-forming controller topology

Table III The Parameters of the Grid-Forming Controller

Parameter	Value	Parameter	Value	Parameter	Value	Parameter	Value	Parameter	Value
H	2 s	K_{pRVI}	5	f_{sw}	4 kHz	T_p	0.01 s	Q_{ref}	0.35 pu
D_{p}	0.03 pu	K_{pLVI}	0	f_0	60 Hz	T_Q	0.01 s	E_{ref}	1.05 pu
D_{q}	0.03 pu	R_{vi0}	0.0	P_{ref}	0.7 pu	T_v	0.01 s	$i_{threshold}$	1.1 pu
K_{p}	0.1	L_{vi0}	0.0	K_{i}	1 s^{-1}	f_{chpf}	0.5 Hz	ω_{ref}	1.0 pu

2.2 Synchronous Machine Model

The SM model available in PSCAD/EMTDC is used with the governor, turbine, and exciter models explained in the subsequent sections. The parameters given in Table IV are used along with the other default parameters.

Table IV The Parameters of Synchronous Machine Model

Parameter	Value	Parameter	Value	Parameter	Value	Parameter	Value
H	2 s	D (Mech. Fric. and Windage)	0.0 pu	$V_{\text{L-N}}$ rms	0.23094 kV	I rms	0.7217 kA

A. SM Governor and Turbine Models

Simplified governor and turbine models are represented by lag compensator blocks with typical time constants [1]. This further enables the SM model in PSCAD/EMTDC to receive the power reference as an input. The implemented governor and turbine topologies are given in Fig. 3. The parameters of

the governor and turbine are given in Table V. The difference between the speed reference (ω_{ref}) and the calculated speed of the SM (ω) is scaled by the droop co-efficient (R_p), and the power reference (P_{ref}) bias is added to create the power input to the governor block. This signal passes through two lag compensator blocks with time constants T_G and T_{CH} representing the governor and the turbine, respectively, to generate the mechanical torque signal (T_M).
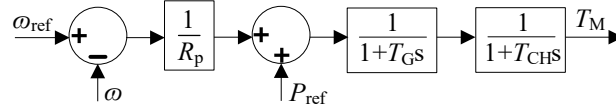
Figure 3 Governor and non-reheat type turbine models of SM

Table V The Parameters of Governor and Non-Reheat Type Turbine Models

Parameter	Value	Parameter	Value	Parameter	Value	Parameter	Value	Parameter	Value
T_G	0.2 s	T_{CH}	0.3 s	R_p	0.03 pu	P_{ref}	0.7 pu	ω_{ref}	1.0 pu

B. SM Exciter Model

The ACA4 exciter model given in Fig. 4 is developed and used with the control parameters given in Table VI. The difference between the expected RMS terminal voltage (v_{ref}) and the measured RMS terminal voltage (v_t) is passed through lead-lag and lag compensator blocks to obtain the required field voltage (E_{FD}). The measured field current (I_{FD}) is considered in defining one of the upper limits.
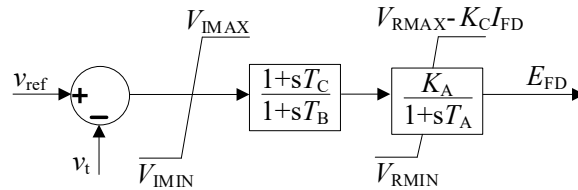

Figure 4 Exciter model of SM

Table VI The Parameters of Exciter Model

Parameter	Value	Parameter	Value	Parameter	Value	Parameter	Value
K_A	200.0	T_B	10.0 s	V_{RMAX}	5.64 pu	V_{RMIN}	-4.53 pu
T_A	0.015 s	T_C	1.0 s	V_{IMAX}	10.0 pu	V_{IMIN}	-10.0 pu
v_{ref}	1.05 pu	K_C	0.0				

3. SIMULATION RESULTS

3.1. Effect of Current Controller on the Fault Response

The role of the VI-based current controller on the fault-ride-through capability of the system is studied under a 50% penetration level from the grid-forming inverter (i.e., VSM and SM are 500 kVA, each). A solid three phase-to-ground fault is applied at the POI for 0.1 s. Firstly, the impact of the current-dependent VI path is analysed by making $R_{\text{vi0}}=L_{\text{vi0}}=0$ pu. Secondly, the transient VI path is activated to observe its added impacts. The following subsections summarise the observations.

A. The impact of K_{pRVI}
K_{pRVI} determines the magnitude of the current-dependent virtual resistance (R_{vi}). The K_{pRVI} is changed in the range of 0-20 and the simulated current contributions from the VSM and the synchronous machine are given in Fig. 5. As expected, when $K_{\text{pRVI}}=0$, the current-limiting action is disabled and the grid forming inverter injects a fault current level of around 4 pu. This violates the 20%-40% overcurrent capability of the power electronic switches [5]. Higher K_{pRVI} values result in lower fault current levels, although very large gain values increase the post-fault oscillations and the reduction in the fault current level is not proportional to the increment of K_{pRVI}. Therefore, in this study $K_{\text{pRVI}}=5$, is selected.
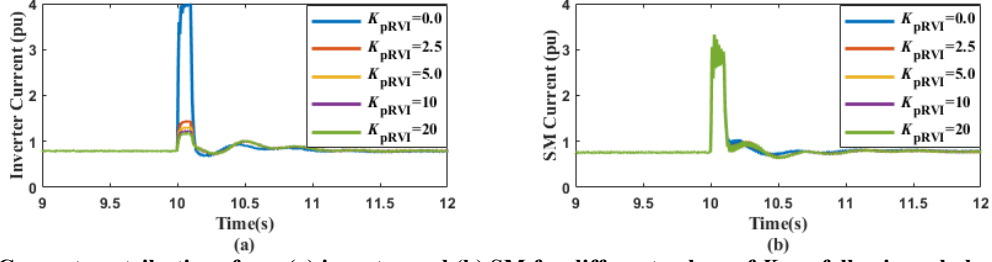
Figure 5 Current contributions from (a) inverter and (b) SM for different values of K_{pRVI} following a balanced fault.

B. The impact of K_{pLVI}

The magnitude of the current-dependent virtual inductance (L_{vi}) is determined by K_{pLVI} gain. Parallel operation and fault current limiting are guaranteed by the VSM control layer and the current-dependent virtual resistance (R_{vi}), respectively. Therefore, L_{vi} is introduced on top of the selected R_{vi} value to observe any potential advantages to improve the fault response. The simulation results confirm that the contribution of L_{vi} is negligible compared to the increment of its value. Without the support of R_{vi}, i.e., with L_{vi} alone, the system cannot recover from the fault. Therefore, $L_{vi}=0$ is used in this experiment to attain the same level of performance with reduced controller complexity.

C. The impact of $I_{threshold}$

$I_{threshold}$ imposes a limit on the inverter current flow. This will, however, not act as a hard limiter; it rather activates the current controller. Therefore, the inverter current passes this threshold and reaches a level slightly higher than the threshold level following an overcurrent situation. The simulation results given in Fig. 6 confirm that $I_{threshold}$ has a significant impact on the peak fault current of the inverter. Lower $I_{threshold}$ values guarantee lower fault current contribution, but values below 1.0 pu cause excessive burden on the normal operation of the inverter. More relaxed thresholds increase the inverter fault current beyond its acceptable level. Considering these factors, $I_{threshold}=1.1$ pu is selected in this study.
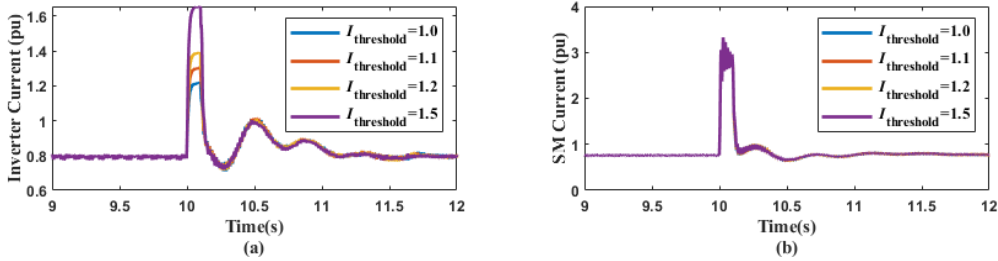

Figure 6 Current contributions from (a) inverter and (b) SM for different values of $I_{threshold}$ following a balanced fault.

D. The impact of R_{vi0}

R_{vi0} introduces a transient virtual voltage drop at the converter terminal following a disturbance to damp out the oscillations in the inverter current. With the selected high-pass filter cut-off frequency of 0.5 Hz, the inverter current oscillations damp out more with higher R_{vi0} values. This occurs at the expense of increased oscillations in the other measurements. Fig. 7 depicts the variations of the current injections and rotational speed deviations following a solid balanced fault. To avoid unwanted post-fault oscillations R_{vi0} is set at zero.

E. The impact of L_{vi0}

L_{vi0} creates a virtual voltage drop proportional to the high frequency component of the inverter current; it is unable to introduce additional damping to post-fault oscillations. Instead, it increases the oscillations after a certain L_{vi0} level. Therefore, $L_{vi0}=0$ is used for the rest of the studies.

F. The impact of f_{hp}

To further explore possible support from the transient VI path, R_{vi0} is set at 0.25 pu and high-pass filter cut-off frequency is changed from 0.5 Hz to 10 Hz. The simulation results (not shown) verify that higher cut-off frequencies lower the post-fault oscillations. This suggests that lower contributions from

4

the transient VI path improve the fault-recovery in the tested conditions. Therefore, both R_{vi0} and L_{vi0} are kept at zero to disable the transient VI path. The transient VI path does not provide additional advantages in these tested conditions. However, in test conditions that create high frequency oscillations, the transient VI path can be used as an active damping method [6].
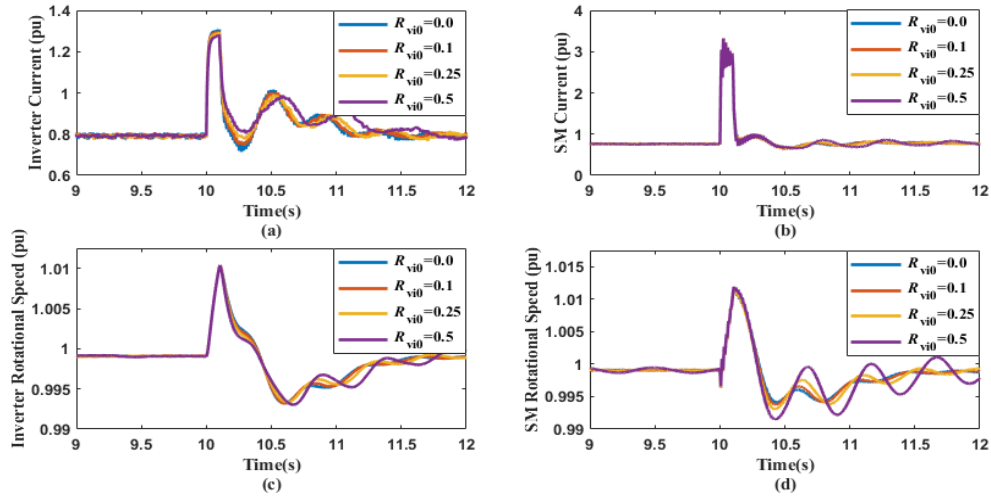

Figure 7 Current contributions from (a) inverter, (b) SM and the rotational speed of (c) inverter, (d) SM for different values of R_{vi0} following a balanced fault.

3.2. Effect of the VSM Dynamics on the Fault Response.

The *P-f* and *Q-v* control paths constitute the main VSM control layer. It can be shown that the time constants are $2HD_p$ [1] and $1/K_i$ for *P-f* and *Q-v* controllers, respectively, where H is the VSM's inertia time constant, D_p is the VSM's *P-f* droop co-efficient, and K_i is the integrator gain of the PI controller. The effect of these VSM's parameters on the fault-ride-through capability of a parallelly connected grid-forming inverter and a SM is studied in the following sub-sections.

A. The impact of H
As the inertia time constant of the VSM can be set arbitrarily, its value is changed in the range 0.5-4.0 s, while all the other parameters are set at the previously mentioned values. Fig. 8 shows the ability of the considered system to ride through a fault with different emulated inertia time constants.

High virtual inertia time constants increase the aggregate inertia time constant of the test system. Therefore, post-fault rotor overshoots have retarded as expected. Further, post-fault oscillations have sustained for a longer period of time with virtual inertia time constants that are close to or larger than the that of the SM (i.e., H_{SM}=2 s).

B. The impact of D_p
The *P-f* droop co-efficient, D_p, is another parameter that determines the response time of the VSM. D_p of the VSM is changed from 0.015 pu to 0.06 pu while keeping D_p of SM at 0.03 pu and the simulation results are given in Fig. 9. The fault-ride-through capability is preserved with the tested D_p values. The increment of the VSM's D_p increases the aggregate D_p of the system; therefore, the post-fault oscillation's period has increased.
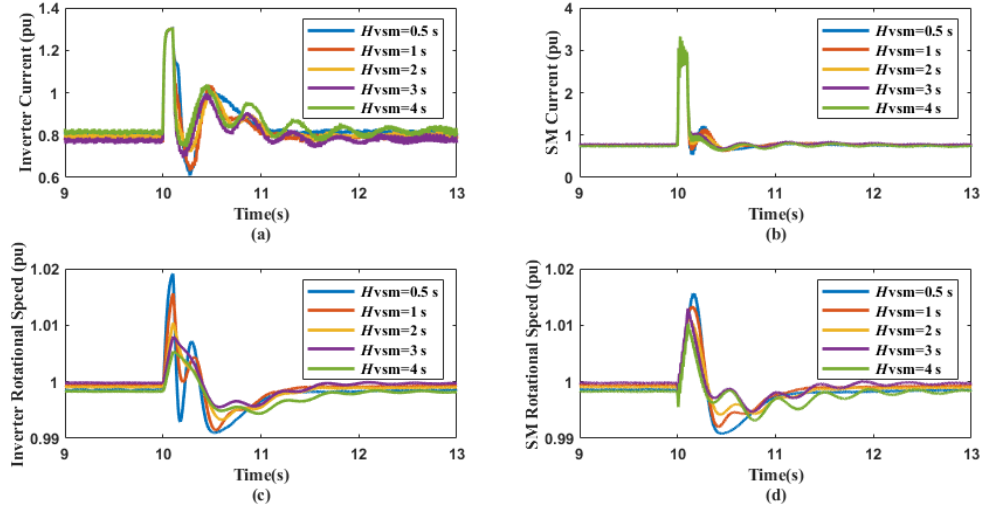
5

Figure 8 Current contributions from (a) inverter, (b) SM and the rotational speed of (c) inverter, (d) SM for different values of H

C. *The impact of K_i*

The time constant of the PI controller is determined by $1/K_i$. Therefore, higher K_i values lead to faster Q-v control of the inverter and vice versa. Fig. 10 shows the simulation results obtained for different K_i values. As shown, slower Q-v controllers take longer to reach the steady state and faster Q-v controllers result in higher post-fault reactive power injections by the VSM. Therefore, in this study K_i=1 is used to reach the steady state within a reasonable time and to avoid large reactive power excursions.
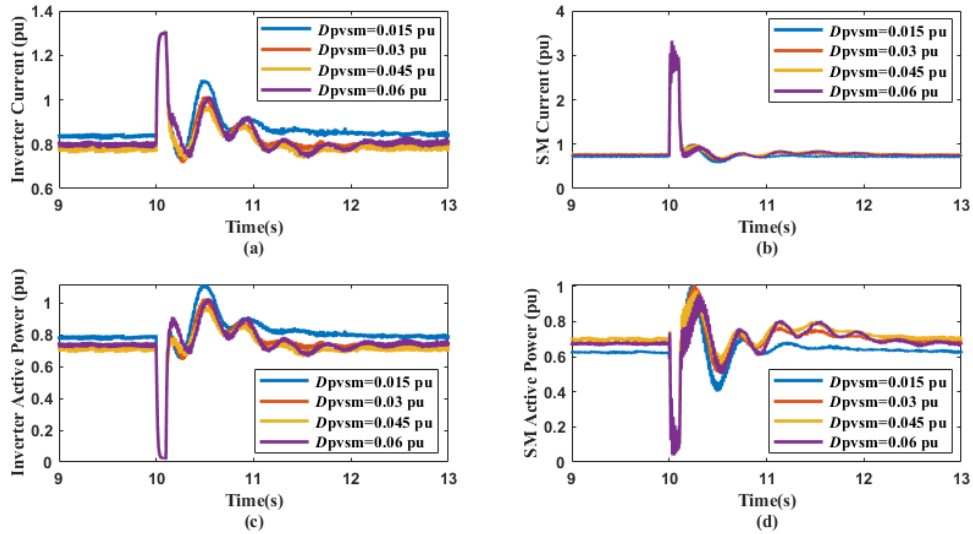

Figure 9 Current contributions from (a) inverter, (b) SM and the active power generation from (c) inverter, (d) SM for different values of D_p
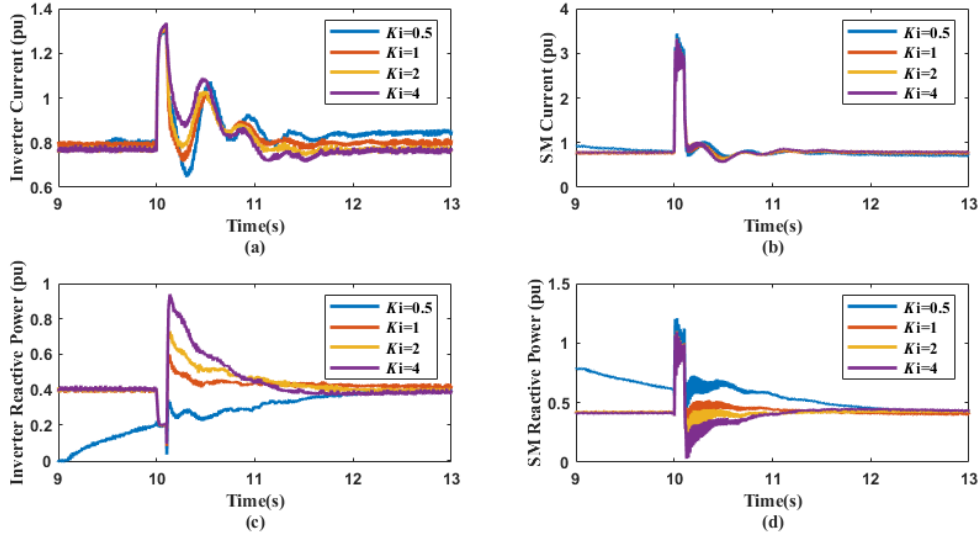
Figure 10 Current contributions from (a) inverter, (b) SM and the reactive power generation from (c) inverter, (d) SM for different values of K_i

3.3. *Effect of the grid-forming inverter penetration level on the fault response*

The sizes of VSM and SM are changed as shown in Table VII while keeping the total generation at 2.4 MW, R_{load} =72.04 Ω, and L_{load} =0.3821 H. Depending on the size of each machine, the corresponding transformer size is scaled. The LCL filter parameters are also re-tunned according to the size of the grid-forming inverter.

Table VII The Sizes of VSM and SM to Create Different Inverter Penetration Levels

VSM:SM ratio	25%	33.3%	50%	66.6%	75%
VSM size (kW)	600	800	1200	1600	1800
SM size (kW)	1800	1600	1200	800	600

The simulation results, which are given in Fig. 11, show the ability of the parallel-connected gird-forming inverter and a SM to feed the load and maintain a promising fault-ride-through capability even under high levels of inverter penetration.
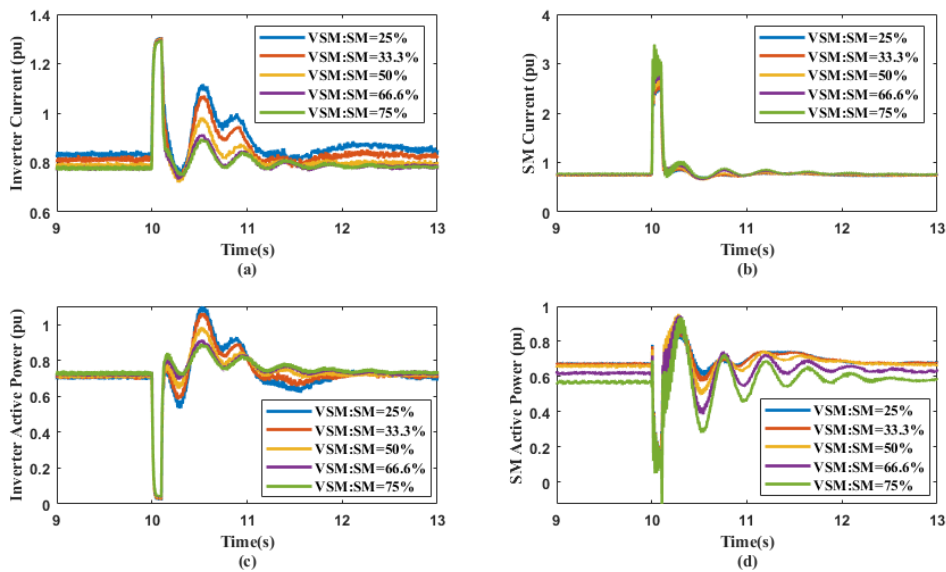

Figure 11 Current contributions from (a) inverter, (b) SM and the active power generation from (c) inverter, (d) SM for different VSM penetration levels

7

3.4. *Effect of the electrical distance between VSM and SM*

The length of the transmission line that connects the VSM to the POI is changed from 2.5 km to 20 km, while keeping the SM 10 km away from the POI. The simulation results in Fig. 12 shows the ability of the test system to ride through a fault with inverter feeding the load from different electrical distances. The simulation results further confirm that the change in the transmission line length has only created different V-*i* droop characteristics according to which the load feeding has been done by each machine and any other impact during and after the fault responses are negligible.
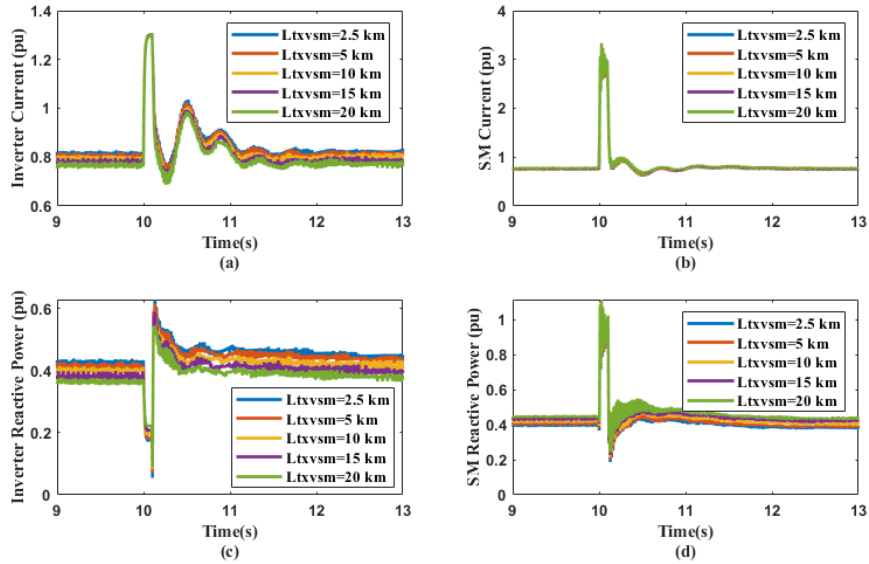

Figure 12 Current contributions from (a) inverter, (b) SM and the reactive power generation from (c) inverter, (d) SM for different transmission line lengths for VSM.

4. CONCLUSIONS

The system studied in the paper replicates a practical application of the parallel operation of a grid-forming inverter with a SM, which can also resemble the Thevenin voltage source equivalent of an external grid. The simulation results show the robustness of the controller in parallel operation and fault-ride-through subjected to the limited current carrying capability of the IGBTs. Tighter current limiting can be created by higher K_{pRVI} and lower $i_{threhsold}$ values; however, such stiff current-limiting methods lead to high post-fault oscillations, which might be more prominent with weaker grid interconnections. The current limiting VR path is the sole factor in determining of the inverter's peak fault current, while all the other VSM's factors and network conditions will only come into action in the post-fault transient duration.

BIBLIOGRAPHY

[1]   P. Kundur, *Power System Stability and Control*, McGraw-Hill, Inc., 1994.
[2]   F. Gao, M. R. Iravani "A Control Strategy for a Distributed Generation Unit in Grid-Connected and Autonomous Modes of Operation," *IEEE Transaction on Power Delivery*, pages 850-859, April 2008.
[3]   A. J. Roscoe, M. Yu, A. Dyśko, C. Booth, R. Ierna, J. Zhu, H. Urdal "A VSM (Virtual Synchronous Machine) Convertor Control Model Suitable for RMS Studies for Resolving System Operator / Owner Challenges " in Proc. Wind Integration Workshop, November 2016.
[4]   A. D. Paqutte, D. M. Divan "Virtual Impedance Current Limiting for Inverters in Microgrids with Synchronous Generators," *IEEE Transaction on Industry Applications*, pages 1630-1638, March/April 2015.
[5]   T. Qoria, F. Gruson, F. Colas, X. Kestelyn, X. Guillaud "Current Limiting algorithms and transient stability analysis of grid-forming VSCs," *Electric Power Systems Research*, 2020.
[6]   S. D'Arco, J. A. Suul, O. B. Fosso "A Virtual Synchronous Machine implementation for distributedcontrol of power converters in SmartGrids," *Electric Power Systems Research*, 2015.